Optik - International Journal for Light and Electron Optics 181 (2019) 562–570

Contents lists available at ScienceDirect

Optik

journal homepage: www.elsevier.com/locate/ijleo

Original research article

Channeled spectropolarimetry with increased bandwidth and aliasing reduction

Naicheng Quan[a,b,*], Caiyin You[a], Chunmin Zhang[c,**], Tingkui Mu[c]

[a] School of Materials Science and Engineering, Xi'an University of technology, Xi'an, 710048, China
[b] Key Laboratory of Spectral Imaging technology of Chinese Academy of Sciences, China
[c] Institute of Space Optics, School of Science, MOE Key Laboratory for Nonequilibrium Synthesis and Modulation of Condensed Matter, Xi'an Jiaotong University, Xi'an, 710049, China

ARTICLE INFO

Keywords:
Polarimetry
Channeled spectropolarimeter
Imaging spectropolarimeter

ABSTRACT

A channeled spectropolarimetry with increased bandwidth and aliasing reduction that consists of a high order retarder and a Wollaston prism is presented. It has the advantages of compact, low-cost, static and a measurement speed of the complete spectrally resolved Stokes vector $[S_0(\sigma)\ S_1(\sigma)\ S_2(\sigma)\ S_3(\sigma)]^T$ around 30 ms. Compared with the conventional channeled spectropolarimetry, it can acquire full resolution $S_0(\sigma)$ reconstruction and $S_1(\sigma)$, $S_2(\sigma)$ and $S_3(\sigma)$ reconstruction without errors caused by dominant aliasing between the channels. Besides, the bandwidth of each channel increases by 7/3 times than that of conventional channeled spectropolarimetry. The feasibility of the proposed method is demonstrated by both simulation and laboratory experiments.

1. Introduction

Spectropolarimeter is capable of measuring the spectrally resolved Stokes parameters, $S_0(\sigma)$, $S_1(\sigma)$, $S_2(\sigma)$ and $S_3(\sigma)$. ($S_0(\sigma)$ is the total intensity of the light, while $S_1(\sigma)$ denotes the part of 0° linear polarized light over 90°, $S_2(\sigma)$ for $+45°$ over $-45°$, and $S_3(\sigma)$ for right circular over left circular, σ is spectral variable). These four parameters constitute the Stokes vector **S** that can describe the complete polarization state of light at a given spectral band. Spectropolarimeter has been developed in recent years as a powerful tool for object detection and identification with preferable accuracy, and become a well-recognized technique in many fields, including biomedical diagnosis, environment monitoring, space exploration, remote sensing, and other scientific areas [1–6]. Since the conventional spectropolarimetry usually contains rotating polarization elements or electrically controllable components, it possesses inherent shortcomings of time-consuming measurement process [7]. For the demands on high speed measurement of the spectrally resolved Stokes parameters, various productive strategies have been developed and tested [3]. Among them, the most attractive method with snapshot measurement capability has been channeled spectropolarimetry [8–15].

In channeled spectropolarimetry (CSP), two thick retarders with thickness ratio of 1:2 or 1:3 and an analyzer are incorporated in front of spectrometers to determine the four spectrally resolved Stokes parameters from only a single modulated spectrum that usually contains seven separated channels. Since each channel has a limited channel width, the spectral resolution of each reconstructed Stokes parameters is lower than that of the spectrometer. Besides, aliasing between the channels are inevitable in principle and crosstalk exists when information in the channel exceeding the bandwidth of that channel and spilling over to an

* Corresponding author at: School of Materials Science and Engineering, Xi'an University of technology, Xi'an, 710048, China.
** Corresponding author.
E-mail addresses: quanncx@hotmail.com (N. Quan), zcm@mail.xjtu.edu.cn (C. Zhang).

https://doi.org/10.1016/j.ijleo.2018.10.175
Received 6 September 2018; Accepted 24 October 2018

adjacent channel. If the majority of the bandwidth of the Stokes parameters are greater than the no crosstalk bandwidth limit of CSP, they cannot be accurately reconstructed. Hence, increasing the relative bandwidth or channel interval, which is determined by the thickness ratio of retarders, can reduce crosstalk and subsequently increase the spectral resolution of the reconstructed Stokes parameters [16]. However, to achieve such goal without sacrificing the compact and static advantages of CSP is always the difficulty, few achievements are reported. Craven et al addressed an artifact reduction technique (ART) that can eliminate the aliasing between the adjacent carrier frequency channels and the centerburst [13,17]. Furthermore, because $S_0(\sigma)$ can be isolated for all optical path difference (*OPD*) values, a full resolution $S_0(\sigma)$ reconstruction can be acquired. Since the ART is performed by combining double measurements with oriented the analyzer at two orthogonal directions, it breaks the static characteristic of CSP. Recently, our group presented a novel spectropolarimeter based on liquid crystal variable retarders (LCVR) and Savart polariscope, which can acquire the complete Stokes vector with full-spectral resolution. However, the LCVR needs generating three different retardances to change the channel intervals, which makes the system time assuming and susceptible to temporal misregistration [18].

In this work, we describe a modified channeled spectropolarimetry (MCSP) with improved spectral resolution and aliasing reduction without sacrificing the compact and static advantages of CSP. The dominant aliasing caused by $S_0(\sigma)$ can be eliminated and full resolution $S_0(\sigma)$ reconstruction can be achieved. Besides, the interval between the channels can be increased by 7/3 times than that of CSP, which leads to an improved spectral resolution of reconstructed $S_1(\sigma)$, $S_1(\sigma)$ and $S_3(\sigma)$. Furthermore, MCSP can provide a compact, low-cost, high speed solution and it allows one to measure the four spectrally resolved Stokes parameters in real-time speed. The configuration and theoretical model of the MCSP is described in Section 2. Section 3 compares the performance of MCSP and CSP by simulation. Section 4 presents the laboratory data and discusses the results, while our conclusion is contained in Section 5.

2. Principle

2.1. Optical configuration

The schematic of the proposed MCSP is portrayed in Fig. 1. It has a compact configuration and requires no moving parts to extract the spectrally resolved Stokes parameters. The Stokes vector **S** emitting from the target passes through a high-order retarder R and a Wollaston prism (WP). The spectrum of the exiting light is then recorded by the pair of spectrometers. R is oriented with its fast axis at 22.5° to *x* axis. The WP contains two orthogonally oriented birefringent crystal prisms with optic axes orientations of 0° and 90° with respect to the *x* axis, respectively. The output beam from R is angularly split into two orthogonally polarized beams I_1 and I_2 by WP in the plane perpendicular to *x*-*z* plane. Since the modulated spectrum of I_1 and I_2 are recorded by two separated spectrometers, the WP acts as orthogonal linearly polarizers and the corresponding polarization directions are parallel and perpendicular to x axis, respectively (Tables 1–3).

2.2. Theoretical model

By using the Mueller calculus, the Stokes vector of the emergent light from WP can be described as [8,14]

$$\mathbf{S_{out_1}} = \mathbf{M}_{\mathrm{WP_1}}\mathbf{M}_{\mathrm{R}}\mathbf{S_{in}} \tag{1}$$

$$\mathbf{S_{out_2}} = \mathbf{M}_{\mathrm{WP_2}}\mathbf{M}_{\mathrm{R}}\mathbf{S_{in}} \tag{2}$$

where $\mathbf{M}_{\mathrm{R}}$, $\mathbf{M}_{\mathrm{WP_1}}$ and $\mathbf{M}_{\mathrm{WP_2}}$ are the Mueller matrices of the high-order retarder R and the two orthogonal linearly polarizers, respectively. The spectrometer responds to radiation intensity instead of polarization state, so only the first parameter of $\mathbf{S_{out_1}}$ and $\mathbf{S_{out_2}}$ can be measured. The recorded signal is varied with wavenumber and can be expressed as

$$I_1(\sigma) = \frac{K_1}{2}\left[S_0(\sigma) + \frac{S_1(\sigma)}{2} + \frac{S_2(\sigma)}{2} + \left(\frac{S_1(\sigma)}{2} - \frac{S_2(\sigma)}{2}\right)\cos\varphi - \frac{\sqrt{2}}{2}S_3(\sigma)\sin\varphi\right] \tag{3}$$

$$I_1(\sigma) = \frac{K_2}{2}\left[S_0(\sigma) - \frac{S_1(\sigma)}{2} - \frac{S_2(\sigma)}{2} - \left(\frac{S_1(\sigma)}{2} - \frac{S_2(\sigma)}{2}\right)\cos\varphi + \frac{\sqrt{2}}{2}S_3(\sigma)\sin\varphi\right] \tag{4}$$

These cosinusoidally modulated spectrum are the channeled spectrum that frequently used in the field of frequency-domain

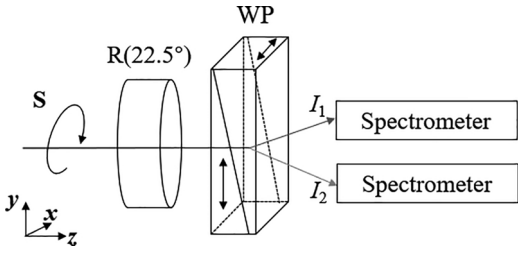

Fig. 1. Schematic of the MCSP.

Table 1
RMSE of derivative of birefringence for single retarders and ARs.

Material	Calcite	$LiNbO_3$	α-BBO	YVO_4	Calcite/YVO_4	$LiNbO_3$/YVO_4	α-BBO/YVO_4
$\Delta q/10^{-3}$	13.90	20.50	6.6	39.5	6.476	1.788	2.061

Table 2
Structure parameters of ARs.

Paring of Materials	Thickness ratio	Thicknesses (mm)
Calcite/YVO_4	2.8	0.37/ 0.11
$LiNbO_3$/YVO_4	1.9	1.01/ 0.53
α-BBO/YVO_4	6.2	4.03/ 0.65

Table 3
RMS error of retardations corresponding to the single retarders and optimal AR.

Material	Calcite	$LiNbO_3$	α-BBO	YVO_4	$LiNbO_3$/YVO_4
RMS error	5.29%	14.53%	3.38%	10.68%	0.85%

interferometry. The phase term is presented as $\varphi(\sigma) = 2\pi\sigma B(\sigma)d$, where $B(\sigma)$ is the birefringence of the crystal, d is the thickness of the retarder R. K_1 and K_2 are amplitude coefficient introduced by the system. Noting that $S_1(\sigma)$, $S_2(\sigma)$ and $S_3(\sigma)$ contained in $I_1(\sigma)$ and $I_2(\sigma)$ display a 180-deg carrier frequency phase shift relative to each other. This enables removal of the channel that contains $S_1(\sigma)$, $S_2(\sigma)$ and $S_3(\sigma)$ when the two spectra are weighted and added

$$I_1(\sigma) + \frac{K_1}{K_2} I_2(\sigma) \propto S_0(\sigma) \tag{5}$$

Eq. (5) is a full-resolution spectrum, as would be collected by the spectrometer that removed the retarder. The aliasing in other channels caused by $S_0(\sigma)$ can be removed by

$$I_1(\sigma) - \frac{K_1}{K_2} I_2(\sigma) \propto S_1(\sigma) + S_2(\sigma) + [S_1(\sigma) - S_2(\sigma)]\cos\varphi - \sqrt{2}\, S_3(\sigma)\sin\varphi \tag{6}$$

Expanding Eq. (6) yields three frequency channels that contain the polarimetric information

$$I_1(\sigma) - \frac{K_1}{K_2} I_2(\sigma) \propto X_0 + X_1 e^{i\varphi} + X_2 e^{-i\varphi} \tag{7a}$$

where

$$X_0 = S_1(\sigma) + S_2(\sigma) \tag{7b}$$

$$X_1 = \frac{S_1(\sigma) - S_2(\sigma) + i\sqrt{2}\, S_3(\sigma)}{2} \tag{7c}$$

$$X_2 = \frac{S_1(\sigma) - S_2(\sigma) - i\sqrt{2}\, S_3(\sigma)}{2} \tag{7d}$$

The inverse Fourier transformation of Eq. (7a) gives an interferogram with the intensity varied with optical path difference:

$$I_1(z) - \frac{K_1}{K_2} I_2(z) \propto [C_0(z) + C_1(z - L) + C_{-1}(z + L)] \tag{8}$$

where z denotes the *OPD* produced by the spectrometer, L is the *OPD* produced by the retarder R. The three components included in $C(z)$, centered at $z = 0, \pm L$ are separated from one another over the *OPD* axis if the retarder thickness is properly selected. These separated channels can be seen from a simulated interferogram shown in Fig. 2, where the input radiation is a broad-band polarization spectrum with the polarization state of $S_0(\sigma)[10.8\ 0.5\ 0.11]^T$. Comparing with CSP, the number of channels is reduced from 7 to 3. For the same total frequency bandwidth supplied by the spectrometer, the bandwidth of each channel is increased by 7/3 times than that of CSP. Filtering channels C_0 and C_{-1} in Eq. (8) and followed by a fast Fourier transform (FFT) enable demodulation of the spectrally resolved Stokes parameters $S_1(\sigma)$, $S_2(\sigma)$ and $S_3(\sigma)$:

$$\Im\{C_0\} \propto S_1(\sigma) + S_2(\sigma) \tag{9a}$$

$$\mathrm{REAL}\{\Im\{C_{-1}\}e^{i\varphi}\} \propto S_1(\sigma) - S_2(\sigma) \tag{9b}$$

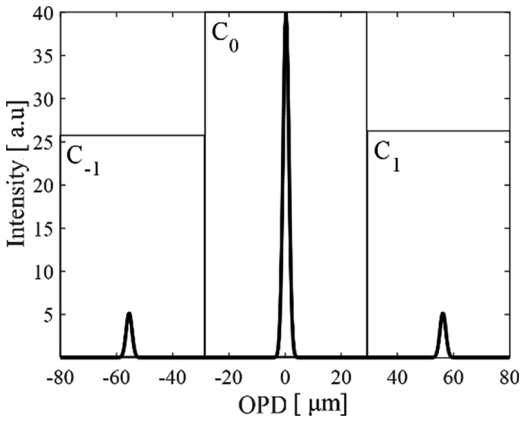

Fig. 2. Simulated interferogram for a broad-band polarization spectrum.

$$\mathrm{IMAG}\{\Im\{C_{-1}\}e^{i\varphi}\} \propto S_3(\sigma) \tag{9c}$$

where $\Im\{\bullet\}$ denotes FFT, REAL$\{\bullet\}$ and IMAG$\{\bullet\}$ denotes taking real and imaginary part operator, respectively.

2.3. Calibration

The proposed MCSP must be calibrated to obtain accurate results. In Eqs. (5) and (6), the recorded spectra $I_2(\sigma)$ is weighted by the ratio of amplitude coefficient K_1/K_2 before being added and subtracted to $I_1(\sigma)$ to determine full spectral resolution $S_0(\sigma)$ and the interference fringe without the dominated aliasing caused by $S_0(\sigma)$ that used to reconstruct the other three Stokes parameters, respectively. K_1/K_2 can be measured by collected two spectra $I_1^u(\sigma)$ and $I_2^u(\sigma)$ corresponding to unpolarized incident light as follows:

$$I_1^u(\sigma) = K_1 S_0(\sigma)/2 \tag{10}$$

$$I_2^u(\sigma) = K_2 S_0(\sigma)/2 \tag{11}$$

$$K_1/K_2 = I_1^u(\sigma)/I_2^u(\sigma) \tag{12}$$

After calibrating K_1/K_2, a full-resolution $S_0(\sigma)$ can be reconstructed directly from Eq. (5). While, $S_1(\sigma)$, $S_2(\sigma)$ and $S_3(\sigma)$ parameters are still modulated by φ as shown in Eq. (6). The phase factor in C_{-1} can be calibrated by using a reference beam with known polarization state [13]. 0° linearly polarized light is selected in MCSP as the reference beam since it can provide large amplitude modulations in the three channels and it yields:

$$e^{i\varphi} = 2\Im(C_{-1}^{0^\circ})/\Im(C_0^{0^\circ}) \tag{13}$$

3. Simulation and discussion

To prove superiority of MCSP over CSP, a simulation experiment is first implemented. The spectral region is 12,500 ~ 25,000 cm^{-1}. The retarders in MCSP and CSP are made of quartz and their birefringence $B(\sigma)$ in the central wavenumber is 0.0096. To illustrate the impact of aliasing on the reconstructed Stokes parameters, noise is not considered in simulation. The thickness of retarder R in MCSP is chosen to be 6.5 mm and the *OPD L* produced by R is 62.55 μm. Thus, the maximum *OPD* of inverse Fourier transformation of Eq. (7a) is $3L/2 = 93.8$ μm. The thicknesses of the two retarders with thickness ratio of 1:2 in CSP simulation can be determined by $\frac{3L}{7B(\sigma)} = 2.78mm$ and $\frac{3L}{7B(\sigma)} = 5.56mm$, respectively. As is shown in Fig. 3(a), narrow-band Stokes vector of $S_0(\sigma)[10.8\ 0.5\ 0.11]^T$ is constructed by Gaussian line shape with an average full width at half maximum of 150 cm^{-1} as the incident light. It is known that the narrower the full width at half-width of the characteristic lines, the wider the bandwidth of channels in CSP required to void crosstalk between the channels [8,16].

Fig. 3(b) shows the Fourier inversion of the modulated spectrum generated by CSP with seven equidistance channels, in which obvious crosstalk exists between channels and distortion of the channel can be observed. By filtering the desire channels and following Fourier transformation in a programed recovery procedure, crosstalk affects the correctness of reconstructed Stokes parameters, which is shown in Fig. 4. Compared with the original spectrum, the reconstructed Stokes parameters have an obvious vibration caused by false crosstalk information and increased full width at half maximum due to the limited bandwidth of each channel. While, Fig. 5 shows the Fourier inversion of the modulated spectrum in Eq. (8). As can be seen, three equidistance channels without crosstalk are separated in *OPD* domain. Since aliasing caused by $S_0(\sigma)$ is removed and the bandwidth of each channel is 7/3 times of CSP, the Stokes parameters reconstructed by MCSP is almost consistent with the incident one, which are shown in Fig. 6.

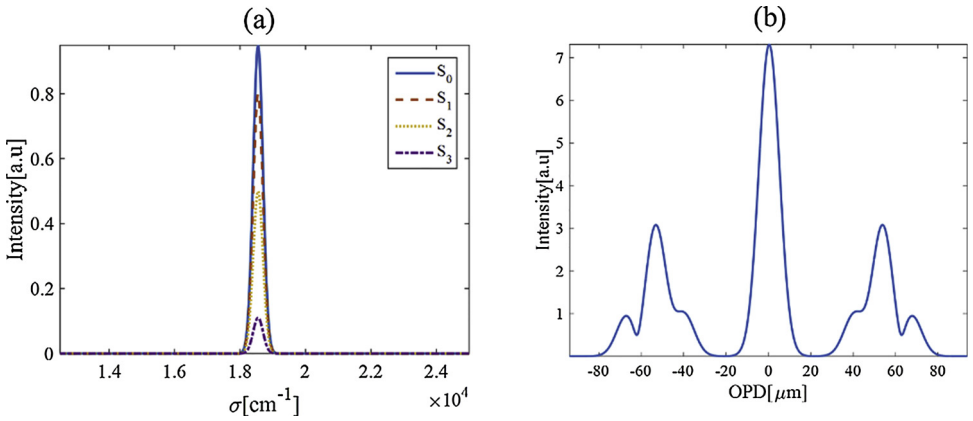

Fig. 3. (a) Narrow-band Gaussian line shape incident polarization spectrum in simulation (b) Fourier inversion of the modulated spectrum generated by CSP with seven equidistance channels.

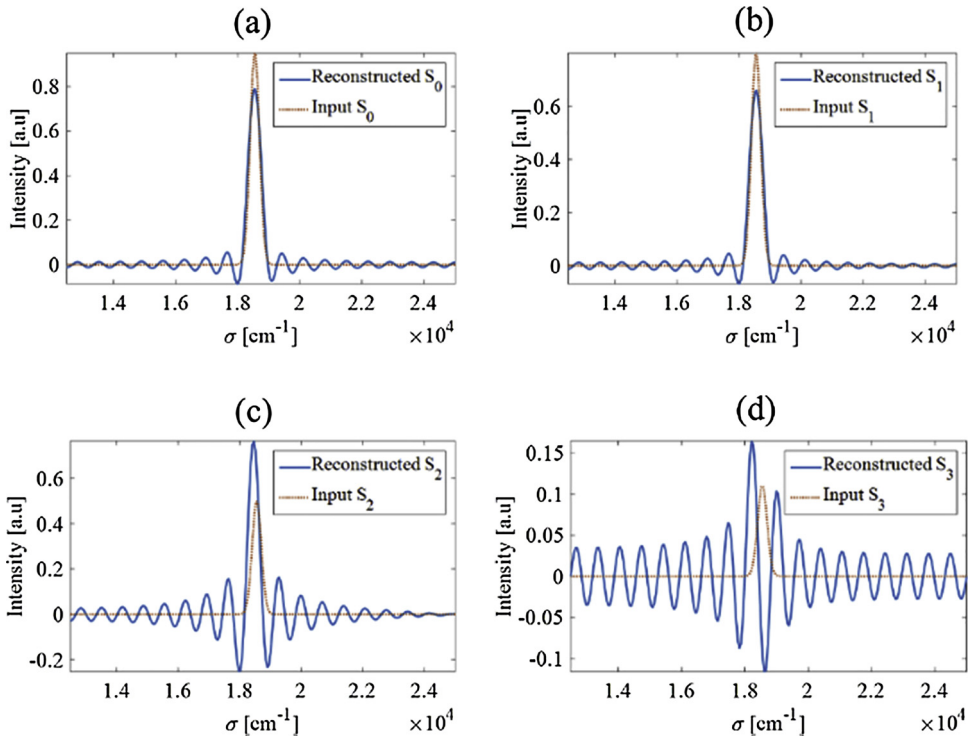

Fig. 4. Spectrally resolved Stokes parameters reconstructed by CSP (a) $S_0(\sigma)$ (b) $S_1(\sigma)$ (c) $S_2(\sigma)$ (d) $S_3(\sigma)$.

4. Experimental results

We carried out a demonstration experiment to prove the feasibility of the proposed MCSP, and the setup is illustrated in Fig. 7. The polychromatic light is conducted to integrating sphere to generate uniform and unpolarized light. A polarization state generator (PSG) consists of different polarization elements is used to generate controllable polarization states. The quartz prism with thickness of 6.5 mm fabricated by Keelaser, Inc is used for the retarder R. The WP is the product of α-BBO prism with splitting angle of 20° supplied by Thorlab, Inc. Spectrum of the light transmitted by WP is recorded with two spectrometers ((FieldSpec3, Analytical Spectral Devices) over the wavenumber range from σ = 12,500 to 25,000 cm^{-1} (wavelength $\lambda = 400 \sim 800$ nm).

In the calibration of the ratio of amplitude coefficient K_1/K_2, we first remove the PSG from the setup. The dual spectra $I_1^u(\sigma)$ and $I_2^u(\sigma)$ are recorded by the two spectrometers. Fig. 8(a) shows the simultaneously captured dual spectra of the unpolarized radiation of halogen-mercury lamp from integrating sphere. Since the spectrometer is preferential to horizontal input, the spectral intensity of $I_1^u(\sigma)$ is stronger than that of $I_2^u(\sigma)$. The ratio of amplitude coefficient K_1/K_2 is show in Fig. 8(b). While, for the calibration of the phase factorφ, a PSG consists of a α-barium borate (α-BBO) Glan-Taylor prism is used to generate 0° linearly polarized light and the

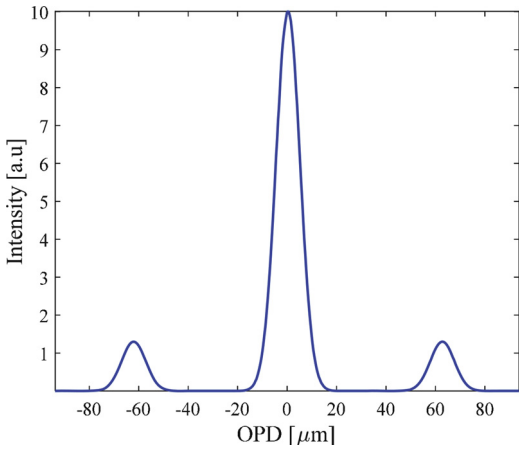

Fig. 5. Fourier inversion of the modulated spectrum generated by MCSP with three equidistance channels.

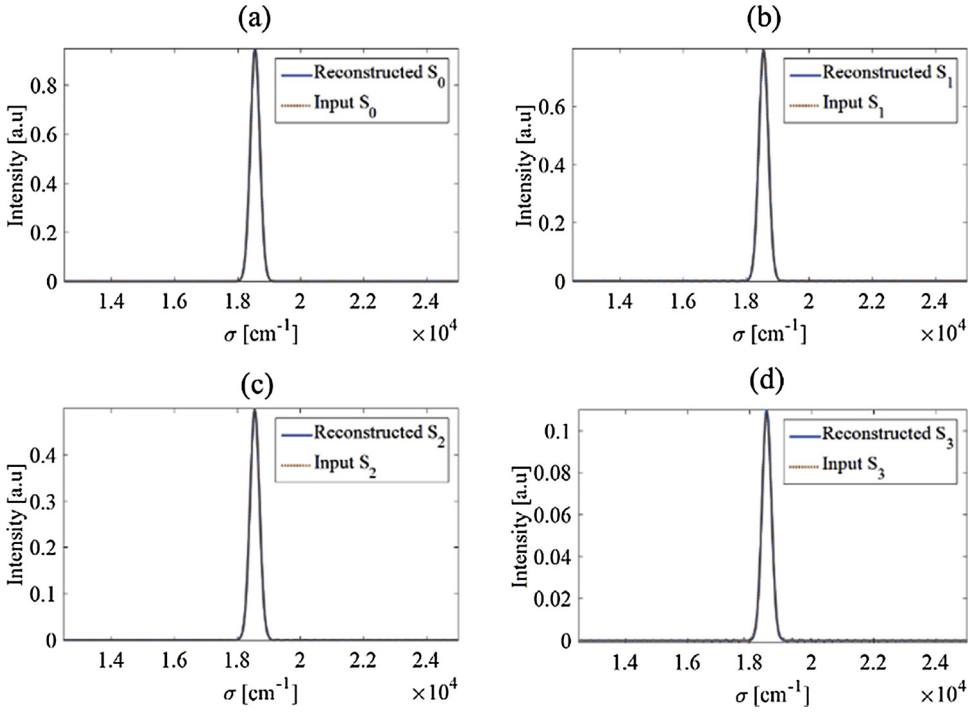

Fig. 6. Spectrally resolved Stokes parameters reconstructed by MCSP (a) $S_0(\sigma)$ (b) $S_1(\sigma)$ (c) $S_2(\sigma)$ (d) $S_3(\sigma)$.

calibrated φ is shown in Fig. 8(c). To verify the results of calibration, the polarization states generated at various rotation angles of the polarizer from 0° to 180° are tested. The reconstructed results of the normalized Stokes parameters obtained as a function of polarizer rotation angle and wavenumber, portrayed in contour plots, can be seen in Fig. 9. Note that the contours of the data in Fig. 9(a) and (b) should ideally consist of straight lines for $S_1(\sigma)$ and $S_2(\sigma)$, the error is increased at the edges of the band due to the low intensity of the input radiation in short wavelength band. Fig. 9(c) can be seen as the error distribution in the reconstruction of $S_3(\sigma)$. The RMS error calculations are performed over the 12,500 ~ 25,000 cm^{-1} (λ = 400 ~ 800 nm) spectral band relative to the known input states, the results show that the average RMS error in each normalized Stokes parameter is given by ξ_{S1}^{rms} = 1.36%, ξ_{S2}^{rms} = 2.13%, ξ_{S3}^{rms} = 1.87%.

Now, the spectrally resolved Stokes parameters measurement of any object is ready. It is known that the conventional CSP can only detect broad-band polarization spectrum. For the spectrum with sharp lines, the channeled interferogram always has a better modulation, which means the intensity of the channeled interferogram decrease slower with the increase of *OPD*.

To verify the feasibility of MCSP on the measuring of spectrum with sharp lines, mercury lamp is chosen to be the light source. By replacing the rotatable polarizer with a PSG consists of a fixed horizontal polarizer and an achromatic quarter wave-plate with fast axes orientations β at 30° and 60° relative to the horizontal, we measure the dual spectra $I_1(\sigma)$ and $I_2(\sigma)$ simultaneously as illustrated

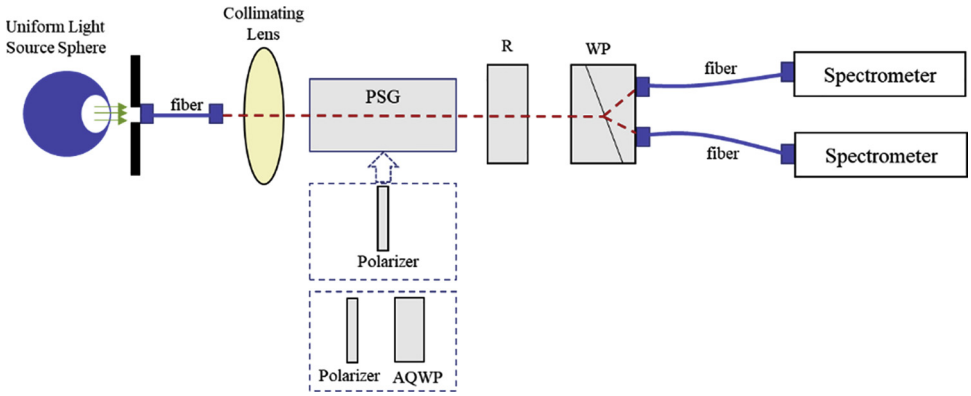

Fig. 7. Experiment setup of MCSP.

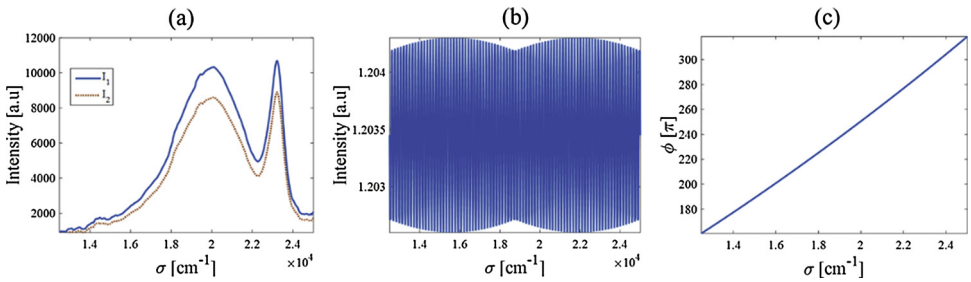

Fig. 8. (a) The recorded dual spectra of unpolarized light (b) the calibrated ratio of amplitude coefficient K_1/K_2 (b) the calibrated phase factorφ.

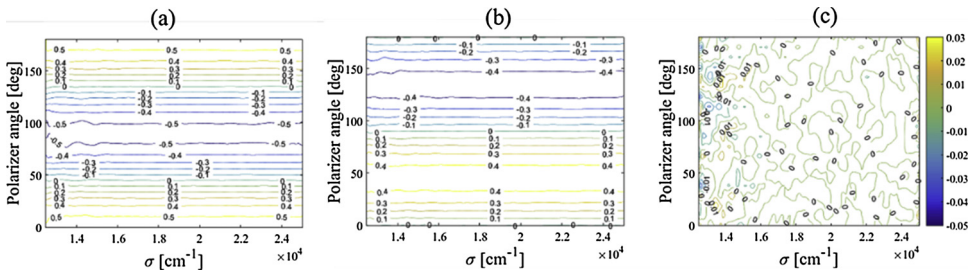

Fig. 9. Contour plots of the reconstructed results for the normalized Stokes parameters (a) $S_1(\sigma)$ (b) $S_2(\sigma)$ (c) $S_3(\sigma)$.

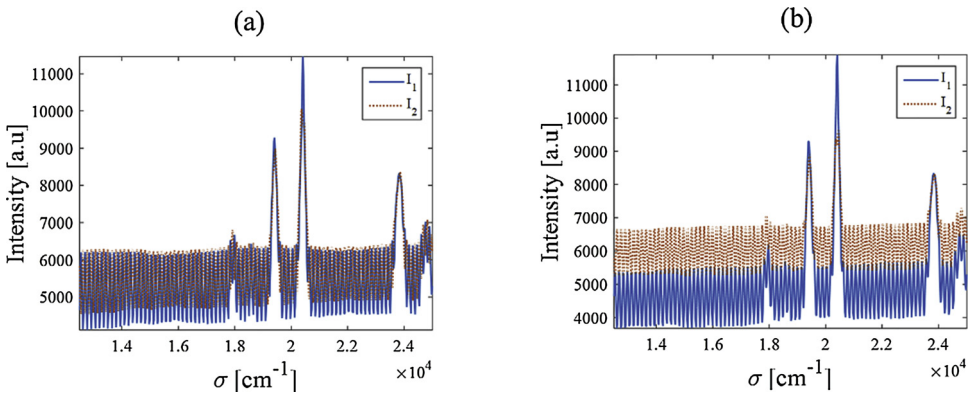

Fig. 10. The measured the dual spectra (a) $\beta = 30^{\circ}$ (b) $\beta = 60^{\circ}$.

in Fig. 10. According to Eq. (7a), Fig. 11 shows the Fourier inversion of the modulated spectrum without $S_0(\sigma)$ aliasing. As can be seen, the three channels are separated completely with equal interval in *OPD* domain. The measurement time of 30 msec suggested in this paper for extracting the spectrally resolved Stokes parameters includes all processing time required for averaging and signal

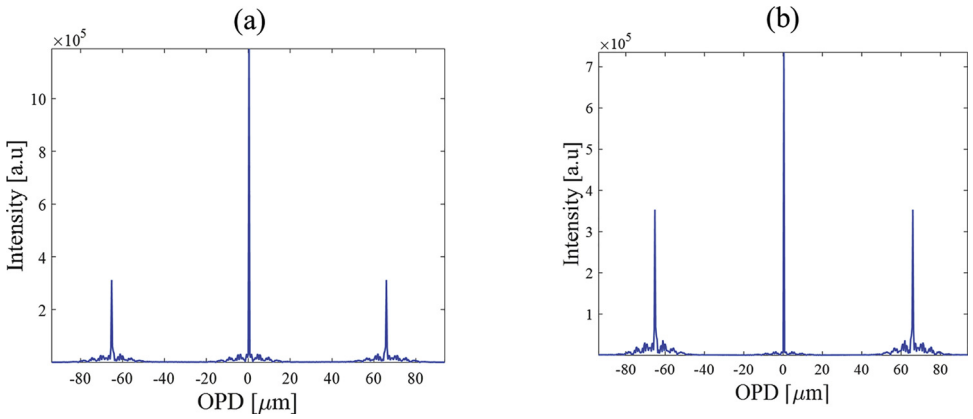

Fig. 11. Fourier inversion of the modulated spectrum without $S_0(\sigma)$ aliasing (a) $\beta = 30^\circ$ (b) $\beta = 60^\circ$.

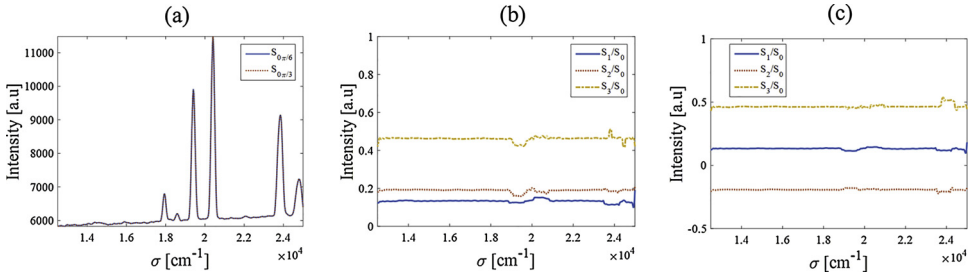

Fig. 12. The reconstructed (a)$S_0(\sigma)$and normalized Stokes parameters (a) $\beta = 30^\circ$ (b) $\beta = 60^\circ$.

processing steps, the reconstructed results are shown in Fig. 12. Since $S_0(\sigma)$ is the total intensity of the light, the reconstructed $S_0(\sigma)$ corresponding to different polarization states is consistent with each other. The curves of the normalized Stokes parameters demonstrate good agreement with the theoretical values in most spectral region, while in some narrow area the curves tend to be fluctuant and deviate from the theoretical values mainly because of the sharp characteristic lines of mercury lamp in this region. Moreover, a slight systematic error can be caused by the signal processing performed in the spectral Fourier domain.

5. Conclusion

In this paper, we present a modified channeled spectropolarimetry (MCSP) consists of a high order retarder and a Wollaston prism (WP) with the advantages of compact, low-cost, high speed solution and the ability to measure complete spectral Stokes vector in real-time speed. Compared with the conventional channeled spectropolarimetry (CSP), the dominant aliasing caused by $S_0(\sigma)$ can be eliminated and full resolution $S_0(\sigma)$ reconstruction can be achieved. Besides, the bandwidth of each channel increases by 7/3 times than that of CSP that can improve the spectral resolution and accuracy of the reconstructed $S_1(\sigma)$, $S_2(\sigma)$ and $S_3(\sigma)$ Stokes parameters. The spectropolarimetric capability are demonstrated by both simulation and laboratory experiments. Further work will install the MCSP to our static interference imaging spectrometer based on Savart polariscope to form a static hyperspectral imaging polarimeter.

Acknowledgments

The authors thank the anonymous reviewers for their helpful comments and constructive suggestions. This work was supported by the Scientific research support program for new teacher of Xi'an University of technology (101-256081706), the Open Research Fund of Key Laboratory of Spectral Imaging Technology, Chinese Academy of Sciences and the National Natural Science Foundation of China (61805193, 41530422, 61775176, 51771145).

References

[1] D.J. Diner, R.A. Chipman, N. Beaudry, B. Cairns, L.D. Food, S.A. Macenka, T.J. Cunningham, S. Seshadri, C. Keller, An integrated multiangle, multispectral, and polarimetric imaging concept for aerosol remote sensing from space, Proc. SPIE 5659 (2005) 88–96.
[2] F. Snik, T. Karalidi, C.U. Keller, Spectral modulation for full linear polarimetry, Appl. Opt. 48 (2009) 1337–1346.
[3] W. Groner, J.W. Winkelman, A.G. Harris, C. Ince, G.J. Bouma, K. Messmer, R.G. Nadeau, Orthogonal polarization spectral imaging: a new method for study of the microcirculation, Nat. Med. 5 (1999) 1209–1212.
[4] T.G. Moran, J.M. Davila, Three-dimensional polarimetric imaging of coronal mass ejections, Science 305 (2004) 66–70.
[5] R.S. Gurjar, V. Backman, L.T. Perelman, I. Georgakoudi, K. Badizadegan, I. Itzkan, R.R. Dasari, M.S. Feld, Imaging human epithelial properties with polarized

light-scattering spectroscopy, Nat. Med. 7 (2001) 1245–1248.
[6] J.S. Tyo, D.L. Goldstein, D.B. Chenault, J.A. Shaw, Review of passive imaging polarimetry for remote sensing applications, Appl. Opt. 45 (2006) 5453–5469.
[7] K. Oka, T. Kato, Spectroscopic polarimetry with a channeled spectrum, Opt. Lett. 24 (1999) 1475–1477.
[8] J.S. Tyo, T.S. Turner, Variable-retardance, Fourier-transform imaging spectropolarimeters for visible spectrum remote sensing, Appl. Opt. 40 (2001) 1450–1458.
[9] S.H. Jones, F.J. Iannarilli, P.L. Kebabian, Realization of quantitative-grade fieldable snapshot imaging spectropolarimeter, Opt. Express 12 (2004) 6559–6573.
[10] R.W. Aumiller, C. Vandervlugt, E.L. Dereniak, R. Sampson, R.W. McMillan, Snapshot imaging spectropolarimetry in the visible and infrared, Proc. SPIE 6972 (2008) D1–D9.
[11] J.C. Jones, M.W. Kudenov, M.G. Stapelbroek, E.L. Dereniak, Infrared hyperspectral imaging polarimeter using birefringent prisms, Appl. Opt. 50 (2011) 1170–1185.
[12] M.W. Kudenov, N.A. Hagen, E.L. Dereniak, G.R. Gerhart, Fourier transform channeled spectropolarimetry in the MWIR, Opt. Express 15 (2007) 12792–12805.
[13] C. Zhang, Q. Li, T. Yan, T. Mu, Y. Wei, High throughput static channeled interference imaging spectropolarimeter based on a Savart polariscope, Opt. Express 24 (2016) 23314–23332.
[14] N. Quan, C. Zhang, T. Mu, Q. Li, Channeled polarimetric technique for the measurement of spectral dependence of linearly Stokes parameters, Infrared Phys. Technol. 90 (2018) 95–100.
[15] D.S. Sabatke, Linear calibration and reconstruction techniques for channeled spectropolarimetry, Opt. Express 11 (2003) 2940–2952.
[16] T. Mu, C. Zhang, Q. Li, L. Zhang, Y. Wei, Q. Chen, Achromatic Savart polariscope: choice of materials, Opt. Express 22 (2014) 5043–5051.
[17] Wong R. Pilkington, A.R. Harvey, Achromatization of Wollaston polarizing beam splitters, Opt. Lett. 6 (2011) 2–1334.
[18] W.J. Tropf, M.E. Thomas, E.W. Rogala, Properties of crystals and glasses, in: M. Bass (Ed.), Chapter 2 in Vol. 4 of Handbook of Optics, 3 ed., McGraw-Hill, New York, 2010, pp. 2.60–2.66.